Applied Catalysis B: Environmental 164 (2015) 151–158

Contents lists available at ScienceDirect

Applied Catalysis B: Environmental

journal homepage: www.elsevier.com/locate/apcatb

Bi^{3+} self doped $NaBiO_3$ nanosheets: Facile controlled synthesis and enhanced visible light photocatalytic activity

Yaobin Ding [a], Fan Yang [b], Lihua Zhu [b,**], Nan Wang [b], Heqing Tang [a,*]

[a] Key Laboratory of Catalysis and Materials Science of the State Ethnic Affairs Commission and Ministry of Education, College of Chemistry and Material Science, South-Central University for Nationalities, Wuhan 430074, PR China
[b] College of Chemistry and Chemical Engineering, Huazhong University of Science and Technology, Wuhan 430074, PR China

ARTICLE INFO

Article history:
Received 5 July 2014
Received in revised form 28 August 2014
Accepted 5 September 2014
Available online 16 September 2014

Keywords:
Sodium bismuthate
Self dope
Visible light photocatalysis
Degradation
Pollutants

ABSTRACT

A facile controlled synthesis method of Bi^{3+} self doped $NaBiO_3$ nanosheets was developed by using acidic hydrolysis of $NaBiO_3{\cdot}2H_2O$ in HNO_3 solutions. It was found that the hydrolysis of $NaBiO_3{\cdot}2H_2O$ in HNO_3 solutions at low concentrations ($0 < c(HNO_3)/c(NaBiO_3{\cdot}2H_2O) \leq 0.2$) resulted in the doping of $NaBiO_3$ nanosheets by Bi^{3+}. In comparison with the untreated $NaBiO_3{\cdot}2H_2O$, the Bi^{3+} self doped $NaBiO_3$ nanosheets prepared at $c(HNO_3)/c(NaBiO_3{\cdot}2H_2O) = 0.2$ were confirmed to show much enhanced photocatalytic activity for the degradation of rhodamine B and bisphenol A under visible light illumination ($\lambda > 420$ nm). The pseudo-zero order reaction kinetic constant for the degradation of rhodamine B (20 $\mu mol\,L^{-1}$) over the Bi^{3+} self doped $NaBiO_3$ was 0.68 $\mu mol\,L^{-1}\,min^{-1}$, being 3.1 times that of $NaBiO_3{\cdot}2H_2O$. The much enhanced photocatalytic activity of the Bi^{3+} self doped $NaBiO_3$ nanosheet photocatalyst was attributed to its improved absorption of visible light and separation of photo-generated h^+/e^- pairs.

1. Introduction

Increasingly serious environmental pollution from hazardous organic compounds is a risk for humanity all over the world, and the efficient treatment of the organic pollutants from the environment is an important issue of the social concerns. Currently used methods for removing organic pollutants from wastewaters include biological, physical, and chemical treatments. In the chemical treatments, photocatalytic technology is known as a promising one because it can mineralize most of organic pollutants by using only luminous energy [1–3]. Among the reported photocatalysts, TiO_2 is the most extensively studied photocatalyst due to its various advantages of low cost, chemical stability and non-toxicity. However, it cannot effectively utilize visible light due to its wide band gap (E_g = 3.0–3.2 eV), which prevents the efficient absorption of sunlight [1]. Appropriate bulky and surface modifications of TiO_2 favor increasing its visible light sensitivity [4,5], but the development of new visible light sensitive non-TiO_2 photocatalysts, such as $BiVO_4$ [6], $BiFeO_3$ [7,8], Ag_3PO_4 [9], has received much more attentions.

Bismuth-based oxides are an attractive group of non-TiO_2 photocatalysts due to their excellent photo-activity arising from the exclusive electron structures [3,6,10]. Generally, a bismuth-based oxide has a narrow band gap with strong visible light absorption and facile hole mobility due to the filled Bi 6s band of Bi^{3+} and empty 6s band of Bi^{5+} [11]. Therefore, several visible light responsive Bi-containing photocatalysts were developed, such as $NaBiO_3$ [11], Bi_2O_3 [12], $BaBiO_3$ [13] and Bi_2WO_6 [14]. For example, Bi_2O_3 can be stimulated by visible light because of its narrow band gap of 2.6–2.8 eV [12]. However, these photocatalysts usually showed low photocatalytic activity due to the high recombination of photo-generated h^+ and e^-. Therefore, it is urgently necessary to develop ways to prepare Bi-containing photocatalysts with high photocatalytic activity.

In order to promote the photocatalytic activity of Bi-containing photocatalysts, several methods were explored as follows. (1) The first one is to construct photocatalysts with a special morphology or exposure of high photoactivity facet, such as Bi_2O_3 nanotubes [15], three-dimensional (3D) BiOCl hierarchitectures [16], and the (0 0 1) facets-dependent BiOCl nanosheets [17]. (2) The second one is to construct bismuth oxide composites with heterojunction structure, such as $BiOCl/Bi_2O_3$ [18], Bi_2O_4/Bi_2O_{4-x} [19], $Bi_2O_3/TiO_{2-x}B_x$ [20], and Bi_2S_3/BiOCl [21]. (3) The third one is to dope bismuth oxides and get hybrid catalysts such as $Na_xBa_yBiO_3$ [22], Sr-Bi_2O_3 [23] and Ti-Bi_2O_3 [24]. Compared to heterogeneous element doping,

* Corresponding author. Tel.: +86 27 67843323; fax: +86 27 67843323.
** Corresponding author. Tel.: +86 27 67843323; fax: +86 27 67843323.
E-mail addresses: lhzhu63@hust.edu.cn (L. Zhu), hqtang62@aliyun.com, tangheqing@mail.scuec.edu.cn (H. Tang).

http://dx.doi.org/10.1016/j.apcatb.2014.09.019
0926-3373/

self-doping achieves a more homogeneous texture with a merit of preserving the intrinsic crystal structure to enhance the visible-light photocatalytic performance.

Sodium bismuthate ($NaBiO_3$) was a pentavalent bismuthate with a band gap of 2.6 eV, being regarded as an alternative attractive visible light driven photocatalyst [11,25]. However, its photocatalytic activity is required to further improve. It was reported that a BiOCl/$NaBiO_3$ composite being prepared in a water-ethanol medium showed an enhanced visible light photocatalytic activity by 50% in comparison with single $NaBiO_3$ [26,27]. In the present work, we developed a facile soft-chemical method to realize the controllable synthesis of Bi^{3+} self doped $NaBiO_3$ nanosheet photocatalyst. By using rhodamine B (RhB) as a model pollutant, the Bi^{3+} self doped $NaBiO_3$ nanosheets were confirmed to exhibit a great enhancement in the photocatalytic activity by 210% in comparison with $NaBiO_3{\cdot}2H_2O$. The photocatalytic mechanism of the Bi^{3+} self doped $NaBiO_3$ nanosheets was elucidated by investigating the influence of the self doping on the optical properties, the separation and transfer of photogenerated electron-hole pairs and the generation of reactive oxygen species during the photocatalysis.

2. Experimental

2.1. Materials and chemicals

$NaBiO_3{\cdot}2H_2O$, HNO_3, Na_2SO_4, RhB, bisphenol A (BPA), tertbutyl alcohol (TBA), p-benzoquinone (BQ) and triethanolamine (TEA) were provided by Sinopharm Chemical Reagent Co., Ltd. (Shanghai, China). All the reagents were of analytical purity and were used as received.

2.2. Preparation of self doped $NaBiO_3$ nanosheets

Bi^{3+} self doped $NaBiO_3$ nanosheets were prepared by the hydrolysis of $NaBiO_3{\cdot}2H_2O$ in HNO_3 aqueous solutions with typical procedures as follows. $NaBiO_3{\cdot}2H_2O$ (0.316 g, 1 mmol) was dispersed in 100 mL of double deionized water during stirring. By adding a certain amount of HNO_3 solution (HNO_3, 0.2 mmol), the hydrolysis of $NaBiO_3{\cdot}2H_2O$ was started. After 30 min for hydrolysis, the resultant solids were separated, washed with double deionized water and finally dried at 100 °C for 8 h, which gave the product of Bi^{3+} self doped $NaBiO_3$ nanosheets. To tune the composition of the prepared samples, different concentrations of HNO_3 were used and the resultant samples were denoted as NBO-*x*, which *x* represented the molar ratio of HNO_3 to $NaBiO_3{\cdot}2H_2O$.

2.3. Characterization

Powder X-ray diffraction (XRD) was conducted on a Bruker Advanced D8 X-ray diffractometer with Cu K_α radiation, operated at 40 mA and 40 kV. Chemical compositions and valence band spectra were analyzed by X-ray photoelectron spectroscopy (XPS) on a Thermo Escalab 250 XPS instrument with a monochromatic Al Ka X-ray source. All binding energies were referenced to the C 1s peak (284.6 eV) arising from adventitious carbon. The morphology and phase composition of self doped $NaBiO_3$ were investigated by scanning electron microscopy (SEM, FEI, the Netherlands) and transmission electron microscopy (TEM, FEI Tecnai G20). Diffuse reflectance spectrum (DRS) was recorded on a Shimadzu UV-2550 spectrophotometer with $BaSO_4$ as reference. The Brunauer–Emmett–Teller (BET) specific surface area was measured at 77 K with a Quantachrome Autosorb-1-C-MS apparatus. The surface area was calculated using BET model for adsorption branch with relative pressure ranging from 0.05 to 0.30.

2.4. Photocatalytic experiments

Photocatalytic activity of the Bi^{3+} self doped $NaBiO_3$ nanosheets was evaluated through the degradation of RhB under the illumination of visible-light ($\lambda > 420$ nm). In the experiment, Bi^{3+} self doped $NaBiO_3$ nanosheets (1.0 g L^{-1}) was dispersed in 50 mL double deionized water containing 20 μmol L^{-1} RhB. The suspension was magnetically stirred in dark for 30 min to ensure adsorption–desorption equilibrium of RhB on the nanosheets prior to illumination. Then the suspension was irradiated under a 500 W halogen tungsten lamp, which was positioned in the middle of the reactor and about 15 cm away from the suspension surface. A 420-nm cutoff was used to ensure the ultraviolet part of illumination was filtered out. At given time intervals, an appropriate amount of the suspension was taken out, and the concentration of residual RhB was analyzed with a spectroscopic method on an UV–vis absorption spectrophotometer (Agilent Technologies cary-60 UV-Vis).

To identify the active species in the photocatalytic process, TBA, BQ or TEA (0.2 mmol L^{-1}) was added into the RhB degradation system as a quencher of hydroxyl radicals (•OH) [28], superoxide radicals ($\bullet O_2^-$) [29] and holes (h^+) [30], respectively.

In order to eliminate any sensitization effect of the dye RhB, the visible light photocatalytic activity of self doped $NaBiO_3$ nanosheets was also evaluated by using 0.1 mmol L^{-1} BPA as a colorless model pollutant, instead of RhB. The concentration of BPA was analyzed with a HPLC (Agilent 1200 infinity series) with a G1315D 12600 DAD detector at a wavelength of 230 nm. An amethyst C18-P column (5 μm, 4.6 mm × 250 mm) was used as separation column. The mobile phase used for HPLC experiments was a mixture of methanol and water (40:60, v/v) and was filtered through 0.2 μm filter prior to use. The flow rate was set at 1.0 mL min^{-1} and the injection volume was 50 μL.

2.5. Photoelectrochemical measurement

Bi^{3+} self doped $NaBiO_3$ nanosheets (20 mg) were dispersed in 5 mL ethanol, and the obtained slurry was then dip-coated onto the surface of a conductive glass electrode (ITO) with a circular exposure area (d = 3.5 mm). After dried at 60 °C for 8 h, the coated ITO electrode was used as the photoanode. By using a platinum sheet and saturated calomel electrode (SCE) as auxiliary electrode and reference electrode, respectively, the photo-generated current was measured on a CHI660 electrochemical workstation (Chenghua, Shanghai) in the electrolyte solution of 0.5 M Na_2SO_4 at a bias potential of 0.1 V under the irradiation of a 300 W xenon lamp with a 420-nm cutoff.

3. Results and discussion

3.1. Catalyst characterization

As shown in Fig. 1a, $NaBiO_3{\cdot}2H_2O$ exhibited a typical flake morphology, consisting of nanosheets with width (length) of ~1.0 μm and thickness of 10–15 nm. The as-prepared NBO-0.2 (Bi^{3+} self doped $NaBiO_3$) sample showed similar morphologies as shown in Fig. 1b and c. It seemed that the nanosheets of the NBO-2 sample (x = 2) were corroded to an extent, and the corrosion became more obvious when the concentration of HNO_3 was further increased (for example, x = 8, Fig. S1b). This hints that a high HNO_3 concentration induces the dissolution of the crystalline $NaBiO_3{\cdot}2H_2O$.

Fig. 2 shows the XRD patterns of NBO-*x* samples. It was found that all the XRD diffraction peaks of the commercial $NaBiO_3{\cdot}2H_2O$ matched well with the hexagonal structure of $NaBiO_3{\cdot}2H_2O$ (JCPDS 30–1161, space group R3, with lattice parameters a = 5.564 Å, c = 15.99 Å, γ = 120°) [11]. When the molar ratio of HNO_3 to

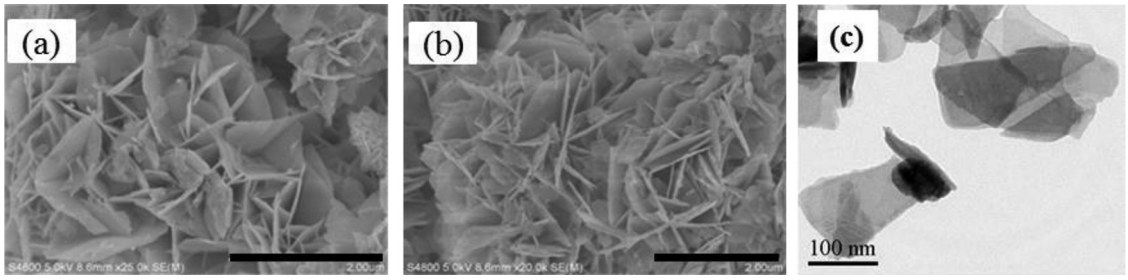

Fig. 1. SEM micrographs of (a) $NaBiO_3{\cdot}2H_2O$ and (b) Bi^{3+} self doped $NaBiO_3$ (NBO-0.2). Scale bar is 2 μm. (c) TEM micrograph of Bi^{3+} self doped $NaBiO_3$ (NBO-0.2).

$NaBiO_3{\cdot}2H_2O$ was controlled at $x = 0.05$ and 0.2, the XRD pattern of the obtained NBO-0.05 and NBO-0.2 showed no obvious changes in comparison with that of $NaBiO_3{\cdot}2H_2O$. For $x > 1$, all the characteristic peaks of $NaBiO_3{\cdot}2H_2O$ became obviously weak, suggesting that the crystal structure of $NaBiO_3{\cdot}2H_2O$ was destroyed. Besides, a new hump peak at $2\theta = 25.7^\circ$, being assigned to bismuth oxide nitrate hydroxide hydrate ($Bi_6O_4(NO_3)_5(OH)_5{\cdot}0.5H_2O$, JCPDS File No. 16-0504) [31], appeared in the XRD pattern of NBO-x ($x \geq 1$, Fig. 2b), indicating that $NaBiO_3{\cdot}2H_2O$ was partly reduced to Bi^{3+} at higher HNO_3 concentrations, which was hydrolyzed into $Bi_6O_4(NO_3)_5(OH)_5{\cdot}0.5H_2O$.

Wide survey XPS spectra of $NaBiO_3{\cdot}2H_2O$ and NBO-0.2 are given in Fig. 3a. Fig. 3b compares the XPS Bi 4f ($4f_{5/2}$ and $4f_{7/2}$) envelops of $NaBiO_3{\cdot}2H_2O$ and NBO-0.2. Typically, the Bi $4f_{5/2}$ (or Bi $4f_{7/2}$) peak could be deconvoluted well into two bimodal peaks at binding energies of 163.6 and 164.5 eV (or 158.2 and 159.4 eV), being attributed to Bi^{3+} and Bi^{5+} [32,33]. According to the deconvoluted spectra, the atomic percentages of Bi^{3+} and Bi^{5+} on surfaces of $NaBiO_3{\cdot}2H_2O$ and NBO-0.2 were estimated. All the Bi species on the surface of $NaBiO_3{\cdot}2H_2O$ were attributed to Bi^{5+}. However, the surface Bi species of NBO-0.2 (Bi^{3+} self doped $NaBiO_3$) consisted of 65.7% Bi^{5+} and 34.3% Bi^{3+}. The O1s XPS envelops of $NaBiO_3{\cdot}2H_2O$ and NBO-0.2 (Fig. 3d) could be deconvoluted into three different peaks at binding energies at 529.5, 531.2, and 533.2 eV, corresponding to the lattice oxygen (Bi—O), chemisorbed oxygen and physically adsorbed oxygen, respectively [33]. Compared with $NaBiO_3{\cdot}2H_2O$, the atomic percentage of the lattice oxygen (Bi—O) on the surface of NBO-0.2 (Bi^{3+} self doped $NaBiO_3$) was much decreased, while that of chemisorbed oxygen and physically adsorbed oxygen was increased accordingly. This indicates that the HNO_3 treatment induced a release of lattice oxygen.

As discussed above, $NaBiO_3{\cdot}2H_2O$ was transformed to Bi^{3+} self doped $NaBiO_3$ and $Bi_6O_4(NO_3)_5(OH)_5{\cdot}0.5H_2O/NaBiO_3$ composite when it was hydrolyzed in aqueous HNO_3 solution. $NaBiO_3$ possess a layered structure, in which BiO_6 octahedra joints each other to form Bi_2O_6 layers carrying negative electrical charges and sodium cations exist between the layers and are exchangeable [34]. Therefore, in the acidic solution, Na ions in $NaBiO_3{\cdot}2H_2O$ were easily released, which destroyed its crystal structure and induced its structural instability, finally inducing the release of O^{2-} ions in the form of oxygen gas and the formation of Bi^{3+} in BiO_6 octahedra. In general, the existence of Bi^{3+} in the $NaBiO_3$ lattice matrix indicates that oxygen vacancies will be generated to maintain the electrostatic balance according to the following equation,

$$4Bi^{5+} + O^{2-} \rightarrow 4Bi^{5+} + 4e^-/\square + O_2 \rightarrow 2Bi^{5+} + Bi^{3+}{-}\square{-}Bi^{3+} + O_2 \quad (1)$$

where the symbol □ represents an empty position originating from the release of O^{2-} ions in the lattice. When the HNO_3 concentration is high enough, the generated Bi^{3+} hydrolyses readily to produce BiO^+, which further reacts with excess NO_3^- to produce $Bi_6O_4(NO_3)_5(OH)_5{\cdot}0.5H_2O$.

The specific surface area and porosity of the as-synthesized samples were investigated by N_2 adsorption and desorption. As shown in Fig. 4, both the N_2 adsorption–desorption isotherms of $NaBiO_3{\cdot}2H_2O$ and Bi^{3+} self doped $NaBiO_3$ (NBO-0.2) corresponded to type IV with a H3 hysteresis loop, suggesting mesoporous features [35]. The corresponding pore-size distributions of the samples were calculated from desorption branch of the nitrogen isotherms by the BJH method. As shown in the inset of Fig. 4, pore distribution range was wide from 3 to 20 nm and was bimodal with a maximum pore diameter of about 3.8 nm and 5.1 nm for $NaBiO_3{\cdot}2H_2O$, and 3.8 nm and 6.1 nm for NBO-0.2, respectively. As the nanosheets do not contain pores, the formation of the bimodal mesoporous structure should result from the stacking of the $NaBiO_3{\cdot}2H_2O$ sheet-like structure. This hierarchical mesoporous structure can provide efficient transport paths for reactants and active sites for the

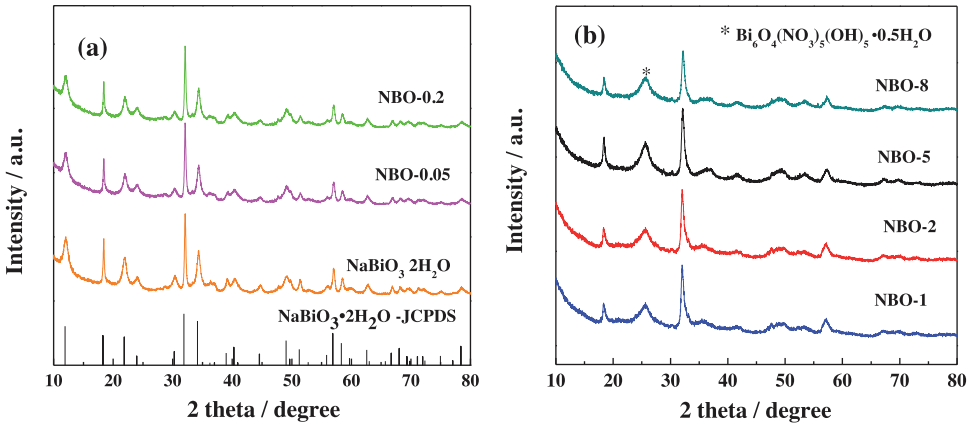

Fig. 2. XRD patterns of NBO-x samples.

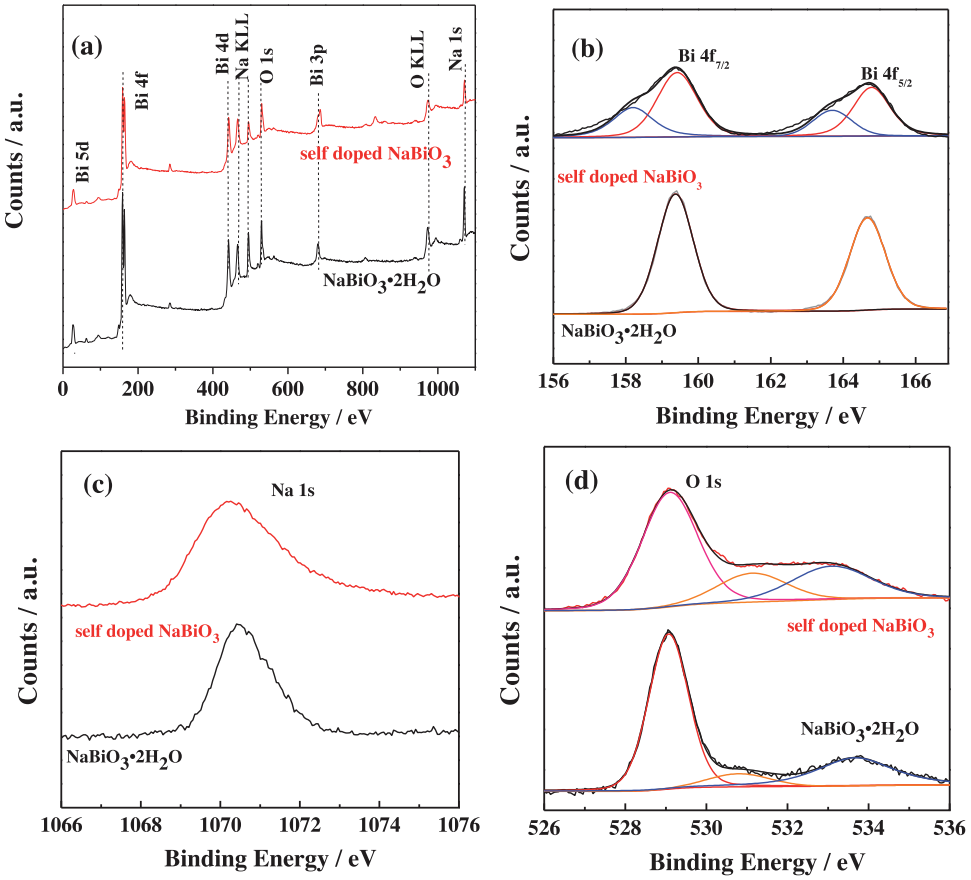

Fig. 3. XPS spectra of $NaBiO_3{\cdot}2H_2O$ and Bi^{3+} self doped $NaBiO_3$ (NBO-0.2): wide survey spectra (a), and high-resolution spectra of Bi 4f (b), Na 1s (c), and O 1s (d).

photocatalytic reaction. The specific surface areas of the NBO-*x* samples were obtained (Table S1), which were little influenced by the acid treatment in the preparation of the NBO-*x* samples. The specific surface area (S_{BET}) of Bi^{3+} self doped $NaBiO_3$ (NBO-0.2) was 36.2 $m^2\ g^{-1}$, being slightly higher than that of $NaBiO_3{\cdot}2H_2O$ with S_{BET} of 32.8 $m^2\ g^{-1}$.

3.2. UV–vis absorption spectra of Bi^{3+} self doped $NaBiO_3$

The UV–vis absorption spectra of NBO-*x* samples were recorded as shown in Fig. 5. Both $NaBiO_3{\cdot}2H_2O$ and NBO-*x* had photoresponses from UV light region to visible light region. Compared to $NaBiO_3{\cdot}2H_2O$, all the NBO-*x* samples had much stronger absorption

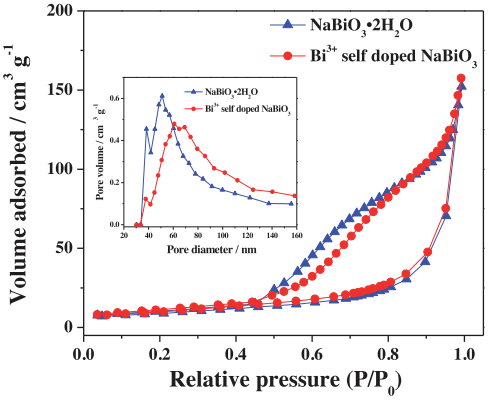

Fig. 4. Nitrogen adsorption–desorption isotherms and the corresponding pore-size distribution curves (inset) of $NaBiO_3{\cdot}2H_2O$ and Bi^{3+} self doped $NaBiO_3$ (NBO-0.2) samples.

in the visible light region with an order of NBO-2 ~ NBO-1 ~ NBO-5 > NBO-0.2 > NBO-8 > NBO-0.05 > $NaBiO_3{\cdot}2H_2O$. This led to their different colors. $NaBiO_3{\cdot}2H_2O$ was pale yellow, while the NBO-*x* samples exhibited yellow, brown, reddish brown and brown when *x* was varied from 0.05 to 8 (Table S1). The NBO-*x* samples showed strong absorption in the region of $\lambda > 600$ nm, probably suggesting that the O defect existed in the crystal structure of NBO-*x* due to the formation of Bi^{3+} [36].

The band gaps (E_g) of $NaBiO_3{\cdot}2H_2O$ and NBO-*x* were calculated according to the following equation,

$$E_g = \frac{1240}{\lambda_g} \quad (2)$$

where E_g is the band gap energy of the semiconductor and λ_g is maximum absorption wavelength. By the calculation, the band gap energy was obtained as 2.45 eV for $NaBiO_3{\cdot}2H_2O$, 2.04 eV for NBO-0.05, 1.68 eV for NBO-0.2, 1.60 eV for NBO-1, 1.58 eV for NBO-2, 1.50 eV for NBO-5, and 1.62 eV for NBO-8, respectively (Table S1). NBO-*x* (with E_g of 1.50–2.04 eV) should be one group of the photocatalysts with the narrowest band gap among the bismuth oxide photocatalysts including $MgBi_2O_6$ (1.8 V) [37], $BiVO_4$ (2.3 eV) [6], Bi_2O_3 (2.8–2.9 eV) [38], $BaBiO_3$ (2.05 eV) [12] and Bi_2WO_6 (2.8 eV) [38]. Therefore, this self doped $NaBiO_3$ photocatalyst is an attractive visible light photocatalyst for pollutant degradation.

3.3. Visible light photocatalytic activity of Bi^{3+} self doped $NaBiO_3$

The photocatalytic activity of $NaBiO_3{\cdot}2H_2O$ and Bi^{3+} self doped $NaBiO_3$ (NBO-0.2) was evaluated by using RhB as a model dye pollutant under visible light ($\lambda \geq 420$ nm) irradiation (Figs. 6 and S2). The visible light photocatalysis in 40 min

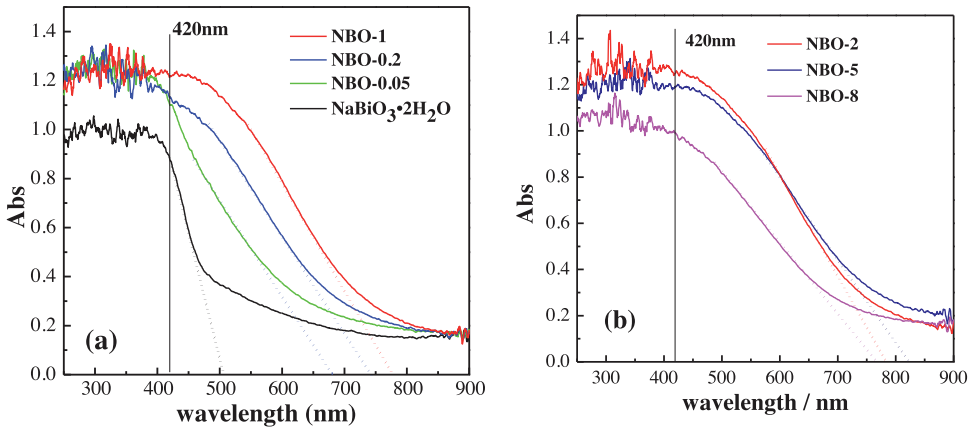

Fig. 5. (a and b) UV–vis DRS spectra of $NaBiO_3{\cdot}2H_2O$ and NBO-*x*.

yielded a decolorization of about 50% of the added RhB over $NaBiO_3{\cdot}2H_2O$, whereas almost all the added RhB was decolorized over Bi^{3+} self doped $NaBiO_3$ (NBO-0.2). The absorption peak of RhB at 553 nm rapidly decreased to zero in 40 min, with concomitant reductions in absorption peaks at 258 nm, 302 nm and 358 nm corresponding to the π–π^* transitions in the RhB (Fig. S2a). This demonstrates the cleavage of the conjugated chromophore and benzene ring. The data of the RhB degradation fitted to a pseudo-zero order reaction model in kinetics. The pseudo-zero order reaction kinetic constant (k) over NBO-0.2 was evaluated as 0.68 $\mu mol\,L^{-1}\,min^{-1}$, being 3.1 times that over $NaBiO_3{\cdot}2H_2O$ (Fig. 6a).

The effect of molar ratio of HNO_3 to $NaBiO_3{\cdot}2H_2O$ (x value) on the photocatalytic activity of the NBO-*x* samples is shown in Fig. 6b. With increasing x value, the rate constant k was increased first, passed a maximum at $x = 0.2$, and then decreased when $x > 0.2$.

In order to rule out the photosensitization process of the Bi^{3+} self doped $NaBiO_3$ photocatalyst (NBO-0.2) in the photodegradation process, BPA, an endocrine disrupting chemical, was chosen as a colorless model organic pollutant. The visible light photocatalytic degradation of BPA (0.1 mmol L^{-1}, 50 mL) was conducted over NBO-0.2 (1 g L^{-1}) similarly (Fig. S3). The direct photolysis of BPA could be neglected, but the photocatalytic degradation of BPA achieved about 55% and 100% in 40 min in the presence of $NaBiO_3{\cdot}2H_2O$ and NBO-0.2 under the visible light irradiation (Fig. S3a). Moreover, the comparison between the photocatalytic activity of NBO-*x* samples toward the BPA degradation (Fig. S3b) demonstrated again that the NBO-0.2 sample showed the best photocatalytic performance among different NBO-*x* samples and the pseudo-zero order reaction kinetic constant (k) of BPA degradation over NBO-0.2 was evaluated as 3.1 $\mu mol\,L^{-1}\,min^{-1}$, being 2.6 times that over $NaBiO_3{\cdot}2H_2O$ (Fig. S3b). This indicates that Bi^{3+} self doped $NaBiO_3$ (NBO-0.2) also show the efficient photocatalytic activity toward colorless organic pollutants.

3.4. Stability and reusability of Bi^{3+} self doped $NaBiO_3$

In the treatment of practical wastewaters, the photocatalyst are required to be stable and reusable. Therefore, the stability and reusability of the Bi^{3+} self doped $NaBiO_3$ were investigated. Firstly, NBO-0.2 (1.0 g L^{-1}) was suspended in a RhB solution (20 $\mu mol\,L^{-1}$). The suspension was magnetically stirred in dark for 30 min to ensure the establishment of adsorption–desorption equilibrium of RhB prior to illumination. After the RhB solution was decolorized by the photocatalytic operation, the reused NBO-0.2 was recycled after filtration, washed with deionized water, and dried at 100 °C for 8 h. The recycled NBO-0.2 was used for the second cycle of RhB degradation. The above procedures were repeated for 10 cycles. As shown in Fig. 7, NBO-0.2 kept high photocatalytic activity after 10 cycles, indicative of its excellent stability and reusability.

3.5. Energy bands of Bi^{3+} self doped $NaBiO_3$

Photocatalytic activity of a semiconductor is closely relevant to its band structure. XPS valence band spectra of the $NaBiO_3{\cdot}2H_2O$ and Bi^{3+} self doped $NaBiO_3$ photocatalysts were recorded to approach their relative band positions. The relative valence band edge of $NaBiO_3{\cdot}2H_2O$ and Bi^{3+} self doped $NaBiO_3$ (NBO-0.2) are both

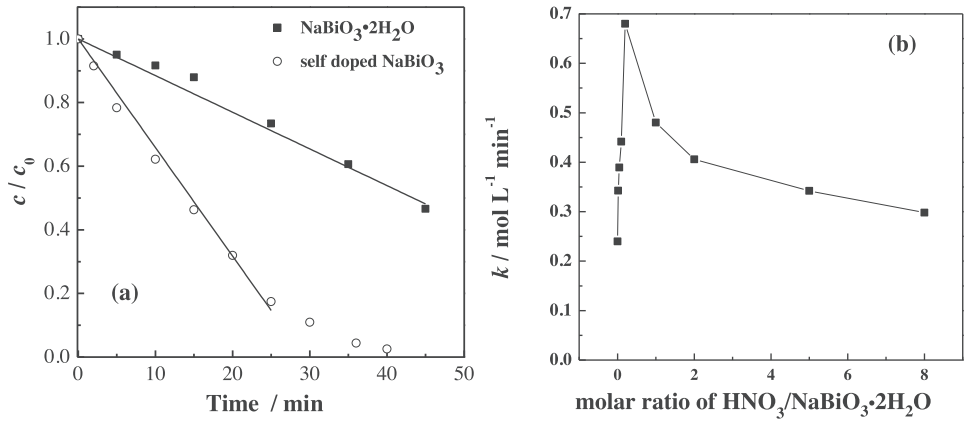

Fig. 6. (a) Photocatalytic degradation kinetics of RhB over $NaBiO_3{\cdot}2H_2O$ and Bi^{3+} self doped $NaBiO_3$ (NBO-0.2). (b) Effects of molar ratio of HNO_3 to $NaBiO_3{\cdot}2H_2O$ on the photocatalytic activity of the NBO-*x* samples.

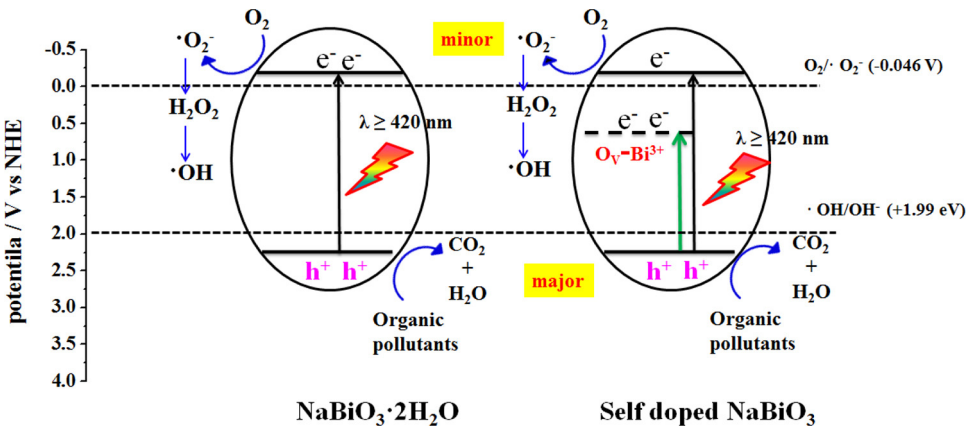

Scheme 1. Energy bands for of $NaBiO_3{\cdot}2H_2O$ and Bi^{3+} self doped $NaBiO_3$ (NBO-0.2).

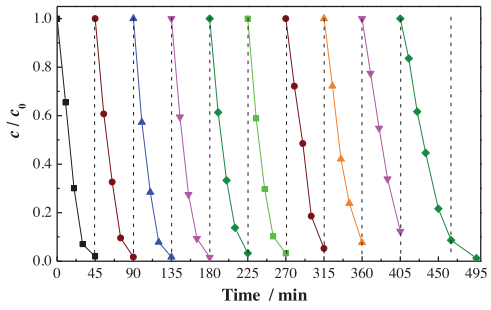

Fig. 7. Photocatalytic stability of the Bi^{3+} self doped $NaBiO_3$ (NBO-0.2).

at 2.25 eV (Fig. S4). It was reported that the highest occupied band corresponding to the broad valence band was mainly composed of O 2p orbitals, while the bottom of the conduction band was identified to be consisted of the hybridized Na 3s and O 2p orbitals [11]. In the non-stoichiometric Bi^{3+} self doped $NaBiO_3$ (NBO-0.2), both contents of Na and O were relatively lower, and Bi^{3+} was introduced into $NaBiO_3$ crystals by replacing Bi^{5+} in BiO_6 octahedra partly with oxygen vacancies generated. These Bi^{3+} defects (abbreviated here as Vo-Bi^{3+}) can produce isolated states in the forbidden gap and act as electron donors. Therefore, the electronic transition from the valence band to Vo-Bi^{3+} is mainly responsible for the enhanced adsorption in the visible light regions. The relative position of energy band of self doped $NaBiO_3$ is proposed in Scheme 1.

3.6. Identification of reactive oxygen radicals

The reactive oxygen radicals in the photocatalytic process were identified by using radical scavenging techniques. TBA can react quickly with •OH, and is often used as a quencher of hydroxyl radicals [28], while the scavenger BQ selectively quenches superoxide radical ($^{\bullet}O_2^-$) in aqueous solution [29]. As shown in Fig. 8a, the addition of excess of either TBA or BQ only slightly decreased the photocatalytic degradation of RhB in both the cases of $NaBiO_3{\cdot}2H_2O$ and NBO-0.2, demonstrating that neither •OH nor $^{\bullet}O_2^-$ was the major reactive species in the concerned systems. However, it was observed from Fig. 8b that the addition of 0.2 mmol L^{-1} TEA, a standard scavenger for photo-generated hole [30], almost completely quenched the photocatalytic decolorization of RhB over both $NaBiO_3{\cdot}2H_2O$ and NBO-0.2. This clearly demonstrates that photo-generated hole is the dominant reactive species responsible for the photocatalytic degradation of organic pollutants over these photocatalysts.

3.7. Mechanism for the enhanced photocatalytic activity of Bi^{3+} self doped $NaBiO_3$

It is well known that high specific surface area, high light absorption ability, suitable energies of valence band (VB) and conduction band (CB), and an efficient charge separation play important roles for the enhancement of photocatalytic activity. As discussed above (Fig. 4 and Table S1), the specific surface area (S_{BET}) of NBO-0.2 was 36.2 m^2 g^{-1}, being only 1.1 times that of $NaBiO_3{\cdot}2H_2O$

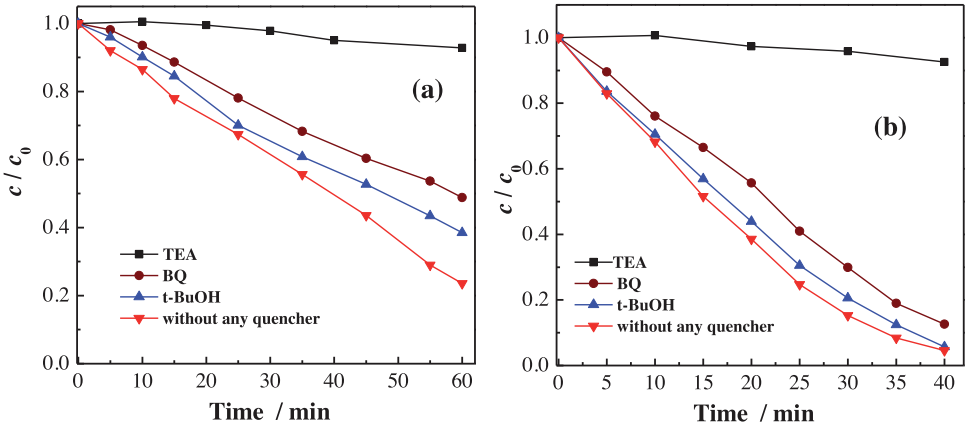

Fig. 8. Effects of TEA (0.2 mmol L^{-1}), BQ (0.2 mmol L^{-1}) and t-BuOH (0.2 mmol L^{-1}) on the photocatalytic degradation of RhB over (a) $NaBiO_3{\cdot}2H_2O$ and (b) Bi^{3+} self doped $NaBiO_3$ (NBO-0.2).

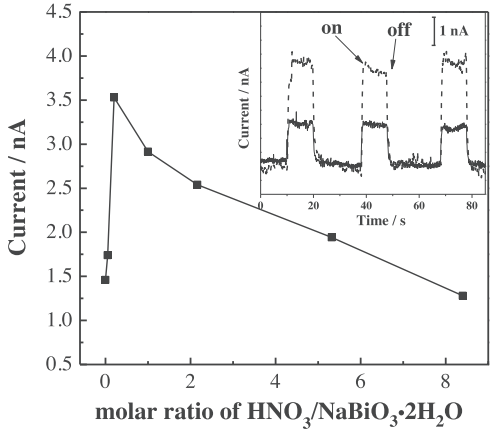

Fig. 9. Effects of the molar ratio of HNO_3 to $NaBiO_3{\cdot}2H_2O$ (x) on the photocurrent responses of NBO-x. The inset is photocurrents of $NaBiO_3{\cdot}2H_2O$ (solid line) and Bi^{3+} self doped $NaBiO_3$ (NBO-0.2) (dash line).

with S_{BET} of 32.8 $m^2\,g^{-1}$. However, the photocatalytic activity of NBO-0.2 toward the RhB degradation was 3.1 times that of $NaBiO_3{\cdot}2H_2O$. This indicates that the increase of S_{BET}, if any, is not the main contributor to the much enhanced photocatalytical activity of Bi^{3+} self doped $NaBiO_3$. The UV–vis absorption spectra of NBO-x showed that the materials had the narrowest band gaps among all the reported Bi-based oxide photocatalysts so far, to our knowledge. This is mainly attributed to the incorporation of Bi^{3+} into $NaBiO_3$ lattice matrix, inducing the formation of Vo-Bi^{3+} isolated states in the forbidden gap. For the surface oxidation reaction, the energy of valence band (VB) of the self doped $NaBiO_3$ is 2.25 eV, being high enough for the oxidation and mineralization of most organic pollutants. As well-known, most of the photo-generated holes and electrons combine in the bulk during their diffusion to the catalyst surface. Therefore, the efficient separation of photo-generated holes and electrons is very important for the design of a highly active photocatalyst. The photocurrent responses of $NaBiO_3{\cdot}2H_2O$ and NBO-x samples were measured under visible light irradiation in the electrolyte solution of 0.5 M Na_2SO_4. As shown in the inset of Fig. 9, the Bi^{3+} self doped NBO-0.2 produced photocurrents being 2.4 times that produced by $NaBiO_3{\cdot}2H_2O$. This photocurrent enhancement suggests that the photo-generated h^+ and e^- in the self doped NBO-0.2 were efficiently separated.

Moreover, the x value was found to have a strong influence on the photocurrent responses of NBO-x (Fig. 9). With increasing x from 0 to 0.2, the photocurrent was increased first, passed a maximum, and began to decrease when $x > 0.2$. Although some NBO-x samples ($x = 1$–5) showed visible light absorption stronger than NBO-0.2 did (Fig. 5), these samples exhibited easier combination of photo-generated h^+ and e^-, which heavily reduced the amount of photo-generated h^+ available for the degradation of the organic pollutant. This explains why NBO-0.2 is the best photocatalyst among all the NBO-x samples.

4. Conclusions

In summary, this work provided a facile and controllable method for the preparation of Bi^{3+} self doped $NaBiO_3$ photocatalysts. The XRD, XPS, SEM and TEM characterizations confirmed the Bi^{3+} self doped $NaBiO_3$ was obtained from the hydrolysis of $NaBiO_3$ in HNO_3 solutions, when the molar ratio of HNO_3 to $NaBiO_3$ was 0.2. The molar ratio of HNO_3 to $NaBiO_3$ strongly influenced on the photocatalytic performance of the obtained samples, and the Bi^{3+} self doped $NaBiO_3$ prepared at $c(HNO_3)/c(NaBiO_3{\cdot}2H_2O) = 0.2$ showed the best photocatalytic activity. The RhB degradation over Bi^{3+} self doped $NaBiO_3$ photocatalyst (NBO-0.2) followed a pseudo-zero order reaction kinetic with the kinetic constant of $k = 0.68\ \mu mol\ L^{-1}\ min^{-1}$, which was 3.1 times that over $NaBiO_3{\cdot}2H_2O$. The dominant active species in the concerned photocatalytic system were confirmed to be the photo-generated holes in the Bi^{3+} self doped $NaBiO_3$ photocatalysts. The enhanced photocatalytic activity of the Bi^{3+} self doped $NaBiO_3$ was attributed to its remarkable increase in its visible light absorption ability and improved separation of photo-generated holes and electrons. The Bi^{3+} self doped $NaBiO_3$ photocatalysts also showed excellent stability during the photocatalytic degradation of the organic pollutant. Therefore, the Bi^{3+} self doped $NaBiO_3$ nanosheets may be a promising efficient visible light driven photocatalyst for the treatment of organic pollutants.

Acknowledgements

Funding is acknowledged from the National High Technology Research and Development Program of China (863 Program) (Grant No. 2012AA06A304) and the National Science Foundation of China (Grant Nos. 21177044 and 21377169).

Appendix A. Supplementary data

Supplementary data associated with this article can be found, in the online version, at http://dx.doi.org/10.1016/j.apcatb.2014.09.019.

References

[1] M.N. Chong, B. Jin, C. Chow, C. Saint, Water Res. 44 (2010) 2997–3027.
[2] A.Z. Huang, N. Wang, M. Lei, L.H. Zhu, Y.Y. Zhang, Z.F. Lin, D.Q. Yin, H.Q. Tang, Environ. Sci. Technol. 47 (2013) 518–525.
[3] C.S. Pan, Y.F. Zhu, Environ. Sci. Technol. 44 (2010) 5570–5574.
[4] N. Wang, L.H. Zhu, K.J. Deng, Y.B. She, Y.M. Yu, H.Q. Tang, Appl. Catal. B 95 (2010) 400–407.
[5] F. Zuo, K. Bozhilov, R.J. Dillon, L. Wang, P. Smith, X. Zhao, C. Bardeen, P. Feng, Angew. Chem. Int. Ed. 124 (2012) 6327–6330.
[6] S. Tokunaga, H. Kato, A. Kudo, Chem. Mater. 13 (2001) 4624–4628.
[7] W. Luo, L. Zhu, N. Wang, H. Tang, M. Cao, Y. She, Environ. Sci. Technol. 44 (2010) 1786–1791.
[8] J. An, L. Zhu, N. Wang, Z. Song, Z. Yang, D. Du, H. Tang, Chem. Eng. J. 219 (2013) 225–237.
[9] Y. Bi, S. Ouyang, N. Umezawa, J. Cao, J. Ye, J. Am. Chem. Soc. 133 (2011) 6490–6492.
[10] K. Zhao, L.Z. Zhang, J.J. Wang, Q.X. Li, W.W. He, J.J. Yin, J. Am. Chem. Soc. 135 (2013) 15750–15753.
[11] T. Kako, Z.G. Zou, M. Katagiri, J.H. Ye, Chem. Mater. 19 (2007) 198–202.
[12] Y. Qiu, M. Yang, H. Fan, Y. Zuo, Y. Shao, Y. Xu, X. Yang, S. Yang, CrystEngComm 13 (2011) 1843–1850.
[13] J.W. Tang, Z.G. Zou, J.H. Ye, J. Phys. Chem. C 111 (2007) 12779–12785.
[14] C. Zhang, Y.F. Zhu, Chem. Mater. 17 (2005) 3537–3545.
[15] L. Li, Y.W. Yang, G.H. Li, L.D. Zhang, Small 2 (2006) 548–553.
[16] L.P. Zhu, G.H. Liao, N.C. Bing, L.L. Wang, Y. Yang, H.Y. Xie, CrystEngComm 12 (2010) 3791–3796.
[17] L.Q. Ye, L. Zan, L.H. Tian, T.Y. Peng, J.J. Zhang, Chem. Commun. 47 (2011) 6951–6953.
[18] S.Y. Chai, Y.J. Kim, M.H. Jung, A.K. Chakraborty, D. Jung, W.I. Lee, J. Catal. 262 (2009) 144–149.
[19] A. Hameed, T. Montini, V. Gombac, P. Fornasiero, J. Am. Chem. Soc. 130 (2008) 9658–9659.
[20] K. Su, Z.H. Ai, L.Z. Zhang, J. Phys. Chem. C 116 (2012) 17118–17123.
[21] H. Cheng, B. Huang, X. Qin, X. Zhang, Y. Dai, Chem. Commun. 48 (2012) 97–99.
[22] F. Peng, C.L. Chen, H. Yu, H.J. Wang, J. Yang, Mater. Chem. Phys. 116 (2009) 294–299.
[23] J.F. Niu, S.Y. Ding, L.W. Zhang, J.B. Zhao, C.H. Feng, Chemosphere 93 (2013) 1–8.
[24] L.F. Yin, J.F. Niu, Z.Y. Shen, J. Chen, Environ. Sci. Technol. 44 (2010) 5581–5586.
[25] K. Yu, S.G. Yang, H. He, C. Sun, C.G. Gu, Y.M. Ju, J. Phys. Chem. A 113 (2009) 10024–10032.
[26] X.F. Chang, G. Yu, J. Huang, Z. Li, S.F. Zhu, P.F. Yu, C. Cheng, S.B. Deng, G.B. Ji, Catal. Today 153 (2010) 193–199.
[27] X. Chang, J. Huang, C. Cheng, Q. Sui, W. Sha, G. Ji, S. Deng, G. Yu, Catal. Commun. 11 (2010) 460–464.
[28] Y. Zhang, N. Zhang, Z.R. Tang, Y.J. Xu, Chem. Sci. 3 (2012) 2812–2822.
[29] L.E. Maning, M.K. Kramer, C.S. Foote, Tetrahedron. Lett. 25 (1984) 2523–2526.
[30] L. Zhang, W. Wang, S. Sun, Y. Sun, E. Gao, Z. Zhang, Appl. Catal. B 148–149 (2013) 164–169.

[31] X. Xiao, R. Hu, C. Liu, C. Xing, C. Qian, X. Zuo, J. Nan, L. Wang, Appl. Catal. B 140 (2013) 433–443.
[32] X.J. Wang, Q. Wang, F.T. Li, W.Y. Yang, Y. Zhao, Y.J. Hao, S.J. Liu, Chem. Eng. J. 234 (2013) 361–371.
[33] K. Yu, S. Yang, S.A. Boyd, H. Chen, C. Sun, J. Hazard. Mater. 197 (2011) 88–96.
[34] A. Dias, R.L. Moreira, J. Raman Spectrosc. 41 (2010) 698–701.
[35] P. Madhusudana, J. Ran, J. Zhang, J. Yu, G. Liu, Appl. Catal. B 110 (2011) 286–295.
[36] J. Tang, Z. Zou, J. Ye, Angew. Chem. Int. Ed. 43 (2004) 4463–4466.
[37] H. Mizoguchi, N.S. Bhuvanesh, P.M. Woodward, Chem. Commun. 34 (2003) 1084–1085.
[38] T. Saison, N. Chemin, C. Chanéac, O. Durupthy, V. Ruaux, L. Mariey, F. Maugé, P. Beaunier, J.P. Jolivet, J. Phys. Chem. C 115 (2011) 5657–5666.